

Carbon nanotube mats and fibers with irradiation-improved mechanical characteristics: a theoretical model

J.A. Åström,¹ A.V. Krasheninnikov,² and K. Nordlund²

¹ Centre for Scientific Computing, P.O.Box 405, FIN-02101, Esbo, Finland and

² Accelerator Laboratory, University of Helsinki, P.O. Box 43, FIN-00014, Finland

(Dated: August 11, 2004)

We employ a theoretical model to calculate mechanical characteristics of macroscopic mats and fibers of single-walled carbon nanotubes. We further investigate irradiation-induced covalent bonds between nanotubes and their effects on the tensile strength of nanotube mats and fibers. We show that the stiffness and strength of the mats can be increased at least by an order of magnitude, and thus small-dose irradiation with energetic particles is a promising tool for making macroscopic nanotube materials with excellent mechanical characteristics.

PACS numbers: 62.20Dc, 81.07.De, 61.80.Az

The outstanding mechanical characteristics of individual single-walled carbon nanotubes (SWNTs) suggest that SWNTs can be employed to make a new generation of materials with unique mechanical and electromechanical properties. Unfortunately, the stiffness of as-produced SWNT samples is quite low, since the raw powder-like material is a light but fragile network of entangled SWNTs and amorphous carbon. Thus, the challenge is to make macroscopic SWNT materials which would preserve as much as possible the stiffness and strength of individual nanotubes.

A number of attempts to form such macroscopic nanotube products have been made [1–6]. Nanotube mats [1–3] known also as nanotube bucky paper were produced by purifying and drying SWNT suspensions [1, 2]. Such mats can basically be viewed as a random quasi-two-dimensional network of SWNT bundles in which the tubes are hexagonally packed due to van der Waals (vdW) interactions. However, due to a low density (or correspondingly, high porosity of $\sim 80\%$ [2]) and weak interactions between the bundles, the experimentally measured tensile modulus, strength and strain to failure of the mats have proven to be several orders of magnitude worse [1, 3] than those for individual nanotubes. In addition to nanotube mats, SWNT fibers were produced by the polymer-flow technique [4]. The SWNT fibers, which in contrast to most ordinary carbon fibers could be strongly bent without breaking, had much better mechanical characteristics than nanotube bucky paper, but they were still weak under tension.

In this Letter, we suggest a means for improving mechanical characteristics of SWNT macroscopic forms—mats and fibers. We show that the stiffness and tensile strength of SWNT mats and fibers can be improved by 1-2 orders of magnitude by irradiation with energetic particles due to irradiation-induced inter-tube covalent bonds at the bundle contact areas.

Earlier experiments have demonstrated that such links can be formed between SWNTs within bundles [7, 8]. Bridging of nanotubes by inter-tube bonds was shown

to reinforce the bundles giving rise to a 30-fold increase in the bundle bending modulus [8]. One can expect that links can also appear between SWNTs in *different bundles*. Moreover, irradiation can even result in complete welding of SWNTs [9].

To calculate the mechanical characteristics of the SWNT mats and fibers, we develop a semi-theoretical model in which the input parameters are the microscopic dimensions and stiffness of SWNT bundles, the porosity of the mats and fibers and the density of irradiation-induced links between tubes.

Our model is a generalization and extension of a semi-theoretical method which has been developed for simulations of networks of macroscopic fibers such as glass-fiber felts and ordinary paper. The model is inherently length scale invariant and can therefore be applied at the nanoscale. As we show below, our model reproduces well the experimental data for nanotube mats. Thus, our results are the first demonstration that such macroscopic models can be successfully applied at the nanoscale for quantitative analysis.

Similar to continuum mechanics model applied recently to nanotube mats [10], our model is based on the geometrical Cox model [11], but in contrast to Ref. [10] and other similar models developed mainly for fiber-reinforced composites, our model takes into account the intrinsic porosity and limited connectivity of such networks as textures of mats and fibers. Note that in our formalism both mats and fibers are treated on equal footing, the difference is only in the average tube orientation, sample density and dimensions of the bundles.

SWNT mats (SWNT_m) are three-dimensional deposits of more or less randomly oriented bundles of nanotubes. Such mats are here modelled as being formed by sedimenting flexible bundles in a random and uncorrelated fashion on a flat substrate and with an isotropic orientation distribution. The typical structure of the nanotube mats used in simulations is shown in Fig. 1. For simplicity all bundles have equal length and

width. The bundles are originally straight, horizontal, and deposited from above. Area coverage q is defined as the average number of bundles covering an area of size L^2 , where L is the length of the bundles. When a depositing bundle first comes into contact with a bundle below, it bends down by an angle ϕ from the horizontal plane on both sides of the contact. It can thus come into contact with other bundles, where similar bendings are performed so that the bundle eventually forms a zigzag pattern. When ϕ approaches zero, a mat is simply a pile of straight horizontal sticks, which obviously has a high porosity and a low degree of connectivity between bundles. When ϕ is increased porosity goes down and connectivity increases. In Fig. 1 the dimensionless width of a bundle is $w/L = 0.02$ and $\phi = 0.3$.

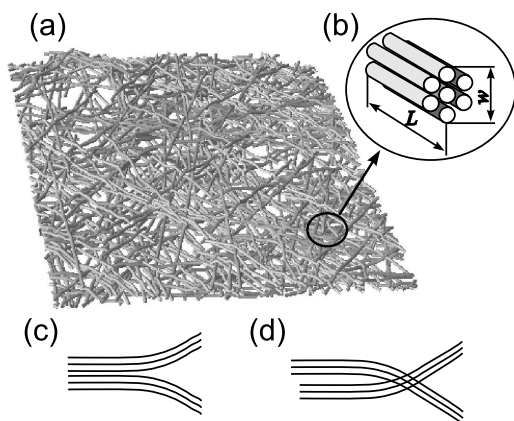


FIG. 1: Typical structure of the nanotube mats used in simulations (a). Schematic representation of a bundle (b). The scale free area coverage is $q = 57$ (see text for details). Schematic representation of bundle branching (c) and crossing (d).

In constructing an effective medium theory of the stiffness of SWNTm we assume that there is no elastic deformation in contacts between bundles. When the force exceeds the critical force, we assume that a contact 'breaks' and slippage takes place. The typical load at which this happens defines the elastic yield point and thus the strength of the SWNTm.

The key parameters in our model are the Young's modulus E and Poisson ratio of the bundles. Also the length and width of the bundles are obviously important. A slightly less obvious yet important parameter is the average number of bundle-bundle contacts per bundle, $\langle n \rangle$. This parameter can be determined through the porosity (or the average density) of the SWNTm.

The porosity of SWNTm relates to the microscopic parameters through

$$\rho = 1 - g\left(\frac{w/L}{\sin(\phi)}\right) \frac{(w/L)^2}{\sin(\phi)}, \quad (1)$$

where L is length of the bundles and w is the width. $g(x)$ is a scaling function that determines $\langle n \rangle$ and

has been calculated numerically[13] through $xg(x) = c_1 \langle n(c_2 x) \rangle \pi/2$ where $c_1 \approx 4.7$ and $c_2 \approx 0.65$.

Now the stiffness (i.e. the effective Young's modulus E_m) of the SWNTm can be determined as

$$E_m \approx \frac{E\pi w \langle n \rangle}{16L} \left[\left(\frac{zw}{l_c} \right)^2 E_1(z) + 3(1 - e^{-z}(z+1)) \right], \quad (2)$$

where $E_n(z) \equiv \int_1^\infty \frac{e^{-zx}}{x^n} dx$ and $l_c/L \approx 3.1(w/L) + 0.18$ [14].

Here $z = l_c \langle n \rangle / L$ where l_c is a fitting parameter roughly proportional to w [14]. A pragmatic consequence of Eq. (2) is that stiffness of SWNTm can e.g. be manipulated by altering the prefactor $E \langle n \rangle (w/L)$ [12].

The deformation stress, σ , of a mat will increase more or less linearly until the mat fails at a tensile strain $\epsilon_c = \sigma_c / E_m$. It is plausible to assume that the sheet fails through slippage at bundle-bundle contacts. The order of magnitude of ϵ_c can be estimated through a simple force balance relation giving

$$\epsilon_c \sim \frac{\tau w \pi \langle n \rangle^2}{2LE_m}, \quad (3)$$

where τ is the tensile strength of a contact. Here we investigate the case when the contact strength originates from not only vdW 'friction' and branching (c.f. Fig. 1c-d) but also covalent bonds between SWNTs. Such bonds can be created by irradiation of the mats or can exist even in pristine samples as a small amount of surface defects can be introduced during the nanotube post-growth processing [15]. Thus, $\tau = f_c \delta$, where f_c is the strength of a bond and δ the area density of such bonds.

As for irradiation-induced bonds, collisions of energetic particles – electrons or ions – with SWNTs give rise to formations of atomic vacancies in the graphitic shells and carbon interstitials in the inter-tube regions. The vacancies can form new vacancy-related defects by saturating some of the dangling bonds [16, 17]. For the single vacancy, this reconstruction results in the appearance of a pentagon ring accompanied by moving of the dangling bond atom out the plane by 0.5-0.7 Å, as in graphite [18]. If there are two vacancies in adjacent tubes (which is frequently the case in irradiated graphitic structures), the protruding atoms can form a covalent bond between the tubes, similar to irradiation-induced bonds in graphite [19].

We employed empirical potential [20] molecular dynamics to simulate the response of SWNTs with irradiation-induced inter-tube links to the mechanical load. We considered two parallel and perpendicular defect-linked tubes in one and the same and different bundles, Fig. 2. The simulation setup was to calculate the critical force that is required to break up the bond between the tubes. We considered two 20-nm-long SWNTs with various chiral indices but roughly the same diameters of 1.2-1.4 nm. Two vacancies in adjacent

shells bridging the tubes were manually created, then the system was relaxed to find out the stable/metastable defect configuration.

In practice, we carried out the bond breaking simulations by applying an external force to the edge atoms of one of the SWNTs. The force grew up linearly with time and the force increase rate varied from 0.001 to 0.03 nN/ps. The atoms at the ends of the other tube were fixed. The simulations were carried out at finite temperatures in the range 0 – 1000 K [22]. Although the bond breaking in such strained systems is a statistical thermally-activated process, we found that the critical force was nearly independent of system temperature. The reason for that is a very big difference between the covalent interaction energy scale (several eV) and the temperature range considered. To avoid the well-known cut-off related overestimate of the maximum force needed to break up a carbon-carbon covalent bond [23], we used increased cut-off values (1.9 and 2.3Å for the lower and upper cutoff ranges, respectively) and interpreted the onset of bond breaking as the moment when the bond length starts fluctuating above the lower cut-off.

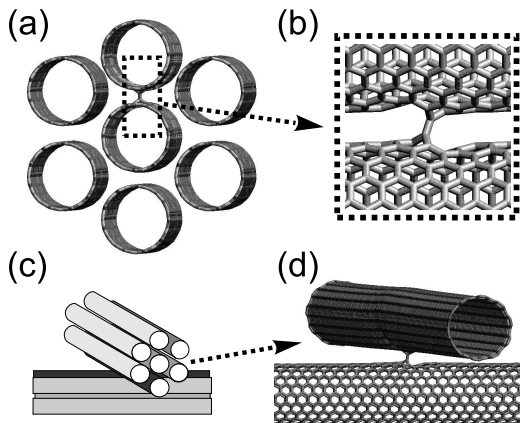


FIG. 2: Molecular models of nanotubes with irradiation-induced covalent bonds. The bond between two parallel nanotubes in the bundle (a,b). The bond between two crossed nanotubes (c,d).

We found that depending on the tube chirality and mutual orientations of the vacancies in the tubes the values of the critical force were in the range of $f_c = 6 - 8$ nN. Below we use $\delta = 2/(1000\text{\AA})^2$ for unirradiated SWNTm, which is about the surface defect density in pristine graphite [24].

Having calculated the microscopic parameters, we proceeded with macroscopic calculation of mat characteristics. We first tested our model (Eq. 2) by calculating the stiffness of computer simulated nanotube mats like the one in Fig. 1.

The stiffness of the computer simulated mats were obtained using a conjugate gradient scheme for the

solution of a set of linear equations. This is a test needed mainly because the numerical functions g and l_c were both obtained for parameter values quite different from those valid for SWNTm. The results are shown in Fig. 3 which displays the stiffness (i.e. 'spring constant') of the virtual mats and the stiffness $E_m A$ where E_m is given by Eq. 2 and A is the effective thickness of the mat. Both are displayed as functions of coverage q for the two set of SWNTm parameter values used below. In Fig. 3A the semi-theoretical model and the simulation results are in excellent agreement outside the percolation critical regime where an effective medium type of model cannot be expected to hold. In Fig. 3B there seems to be an approximately 10% difference outside the critical regime.

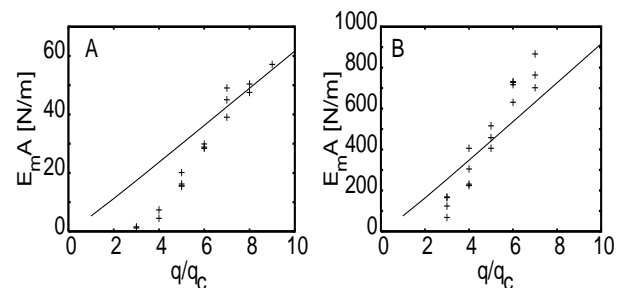


FIG. 3: Stiffness of nanotube mats (i.e. 'spring constant') $E_m A$ where A is the effective thickness of a mat) as functions of coverage q compared with the semi-theoretical estimate through Eq. 2. (a) $w = 10$ nm, $\rho \approx 0.8$, $E = 600$ GPa and $L = 5$ μm . (b) $w = 40$ nm, $\rho \approx 0.3$, $E = 600$ GPa and $L = 5$ μm . Note that the semi-theoretical model cannot be expected to work well close to the percolation critical coverage $q = q_c$. Symbols are conjugate gradient results for different mats and the lines are obtained using Eq. 2.

For further testing we compare the results of our model with two experimental studies of SWNT sheets [1, 3]. In Ref. [1]: $w = 10$ nm, $L =$ 'many micrometers' and $E = 640$ GPa was reported. There is no information about ρ , but in Ref. [10], $\rho \approx 80\%$ for assumingly similar sheets. Using $L = 5$ μm we obtain $E_m \approx 1.4$ GPa which should be compared to $E_m \approx 1.2$ GPa reported in Ref. [1]. A Young's modulus of about 600 GPa is the theoretical value for carbon nanotubes, but experiments have revealed that it might be considerably lower, $E = 200 - 300$ GPa [25, 26]. Using $L = 10$ nm and $E = 200$ GPa we obtain $E_m \approx 0.9$ GPa. That is, E_m is approximately the same as even though E is three times smaller. This is because of the increase in $\langle n \rangle$ due to the longer bundles. Also ϵ_c increases.

In Ref. [3], $w = 40$ nm and $\rho \approx 0.3$ was reported. Using $E = 600$ GPa and $L = 5, 10$ μm we obtain $E_m \approx 4.5, 8.5$ GPa, respectively, which should be compared to $E_m \approx 8$ GPa [3]. The model results for the above parameters give a tensile strain that is about 1%, which is much smaller than the experimentally observed $\epsilon_c \approx 0.35\%$ [3] (notice that we have not counted the initial

| $L_f[\mu\text{m}]$ | $w[\text{nm}]$ | $\rho[\%]$ | $E[\text{GPa}]$ | $E_m[\text{GPa}]$ | $\langle n \rangle$ | $\epsilon_c[\%]$ |
|--------------------|----------------|------------|-----------------|-------------------|---------------------|------------------|
| 5.0 | 10 | 80 | 640 | 1.4 | 7.4 | 0.01 |
| 10.0 | 10 | 80 | 200 | 0.9 | 14.2 | 0.04 |
| 5.0 | 40 | 30 | 600 | 4.5 | 6.5 | 0.01 |
| 10.0 | 40 | 30 | 600 | 8.5 | 12.5 | 0.01 |
| 200.0 | 40 | 30 | 300 | 6.6 | 240 | 0.27 |

TABLE I: Effective medium results for the stiffness of SWNT mats. The input parameters are to the left of the vertical line, and the output parameters are to the right.

non-linear part of the stress-strain curve). This could be explained by e.g. that the value $f_c\delta = 1$ MPa is too low, but it is also possible that L should be larger than $10 \mu\text{m}$, considering that w is four times larger than that in Ref. [1] (compare e.g. with Ref. [4]). Using the values $L = 200 \mu\text{m}$ and $E = 300$ GPa we obtain values comparable with the experimental ones.

The SWNT fibers [4–6] do not have an isotropic orientation distribution – the bundles are aligned along the fiber axis. An estimate based on Cox geometry [11], gives a stiffness increase due to orientation by a factor of 1.3. The high stiffness (7-20GPa) reported in Refs. [4–6] can nevertheless be reproduced by Eq.(2) mainly because of the reported low porosity of the fibers.

We further estimated the upper limit on the stiffness of SWNT mats and fibers exposed to irradiation by energetic particles. Experiments provide convincing evidence for irradiation-mediated improvements of the mechanical characteristics of SWNT bundles [8]. At the same time, the density of inter-bundle covalent bonds would increase. Irradiation should also induce a slight pressure on the bundles and thus press them closer to each other thus decreasing porosity of the sample. As Eqs. 2 and 3 indicate, the stiffness and strength of SWNT mats and fibers are proportional to the stiffness of the bundles and the inter-bundle link density. Thus, one can expect that irradiation should result in the reinforcement of not only individual SWNT bundles, but also macroscopic SWNT materials like nanotube mats and fibers. Specifically, our calculations indicate that the stiffness of nanotube mats and fibers can go beyond 100 GPa after irradiation, assuming optimum irradiation doses, particle types and energies. This is 1–2 orders of magnitude higher than the values reported in Table I. (For example: a 10-fold increase in E and reduction of ρ from 30 to 20 result in a macroscopic stiffness above 100 GPa for the case which has $E_m = 8.5$ GPa in Table I.)

To conclude, we performed macroscopic semi-theoretical calculations of the strength and stiffness of mats and fibers of bundled-up SWNTs. Our model reproduced well the experimentally measured stiffness of macroscopic samples. By employing atomistic microscopic simulations, we further estimated the effects

of irradiation on the tube-tube interface. Finally, using microscopic characteristics as input parameters, we demonstrated that irradiation should result in the reinforcement of not only individual SWNT bundles, but also macroscopic SWNT materials like nanotube mats and fibers. Thus, small-dose irradiation with energetic particles is a promising tool for making macroscopic nanotube materials with excellent mechanical characteristics.

This work was supported in part by the Academy of Finland, Project No. 50578.

-
- [1] R. H. Baughman *et al.*, Science **284**, 1340 (1999).
 - [2] A. Rinzler *et al.*, Appl. Phys. A (Materials-Science-Processing) **67**, 29 (1998).
 - [3] T. V. Sreekumar, T. Liu, S. Kumar, L. Ericson, R. H. Hauge, and R. E. Smalley, Chem. Mater. **15**, 175 (2003).
 - [4] B. Vigolo, A. Penicaud, C. Coulon, C. Sauder, R. Pailier, C. Journet, P. Bernier, and P. Poulin, Science **290**, 1331 (2000).
 - [5] B. Vigolo, P. Poulin, M. Lucas, P. Launois, and P. Bernier, Appl. Phys. Lett. **81**, 1210 (2002).
 - [6] P. Poulin, B. Vigolo, and P. Launois, Carbon **40**, 1741 (2002).
 - [7] H. Stahl, J. Appenzeller, R. Martel, P. Avouris, and B. Lengeler, Phys. Rev. Lett. **85**, 5186 (2000).
 - [8] A. Kis, G. Csányi, J.-P. Salvetat, T.-N. Lee, E. Couteau, A. J. Kulik, W. Benoit, J. Brugger, and L. F6rro, Nat. Mat. **3**, 63 (2004).
 - [9] M. Terrones, F. Banhart, N. Grobert, J.-C. Charlier, H. Terrones, and P. Ajayan, Phys. Rev. Lett **89**, 075505 (2002).
 - [10] T. Liu and S. Kumar, Nano Letters **3**, 647 (2003).
 - [11] H. L. Cox, Br. J. Appl. Phys. **3**, 72 (1952).
 - [12] Graphs of parameter dependencies in Eq. (2) can be found on the AIP’s Electronic Physics Auxiliary Publication Service.
 - [13] J. A. 6rstr6m, M. Latva-Kokko, S. K6hkk6nen, J. P. M6kinen, and J. Timonen, Gran. Matt. **5**, 99 (2003).
 - [14] J. A. 6rstr6m, J. P. M6kinen, M. J. Alava, and J. Timonen, Phys. Rev. E **61**, 5550 (2000); *ibid.* **62**, 5862 (2000); J. Appl. Phys. **88**, 5056 (2000).
 - [15] D. B. Mawhinney, V. Naumenko, A. Kuznetsova, J. T. Yates Jr., J. Liu, and R. E. Smalley, Chem. Phys. Lett. **324**, 213 (2000).
 - [16] P. M. Ajayan, V. Ravikumar, and J.-C. Charlier, Phys. Rev. Lett. **81**, 1437 (1998).
 - [17] A. V. Krasheninikov *et al.* Phys. Rev. B **63**, 245405 (2001); *ibid.* **65**, 165423 (2002).
 - [18] A. A. El-Barbary, R. H. Telling, C. P. Ewels, M. I. Heggie, and P. R. Briddon, Phys. Rev. B **68**, 144107 (2003).
 - [19] R. Telling, C. Ewels, A. El-Barbary, and M. Heggie, Nature Materials **2**, 333 (2003).
 - [20] D. W. Brenner, Phys. Rev. B **42**, 9458 (1990).
 - [21] M. P. Allen and D. J. Tildesley, *Computer Simulation of Liquids* (Oxford University Press, Oxford, England, 1989).
 - [22] The Berendsen temperature control [J. Chem. Phys. **81**, 3684 (1984)] with various time constants (to eliminate

- possible effects of thermostat-system exchange rates on the force) was used to control the temperature.
- [23] T. Belytschko, S. P. Xiao, G. C. Schatz, and R. S. Ruoff, *Phys. Rev. B* **65**, 235430 (2002).
- [24] J. G. Kushmerick, K. F. Kelly, H.-P. Rust, N. J. Halas, and P. S. Weiss, *J. Phys. Chem. B* **103**, 1619 (1999).
- [25] J.-P. Salvetat, G. A. D. Briggs, J.-M. Bonard, R. R. Bacsa, A. J. Kulik, T. Stockli, N. A. Burnham, and L. Forró, *Phys. Rev. Lett.* **82**, 944947 (1999).
- [26] M.-F. Yu, B. S. Files, S. Arepalli, and R. S. Ruoff, *Phys. Rev. Lett.* **84**, 5552 (2000).